Toxicology Research

PAPER

View Article Online
View Journal | View Issue

Cite this: *Toxicol. Res.*, 2018, **7**, 172

Changes in silica nanoparticles upon internalisation by cells: size, aggregation/agglomeration state, mass- and number-based concentrations†

Dorota Bartczak, *[a] Julie Davies,[a] Christian Gollwitzer,[b] Michael Krumrey [b] and Heidi Goenaga-Infante[a]

Monitoring the physicochemical characteristics of nanoparticles following internalisation by cells is a vital step in understanding their biological impact and toxicity. Here, the feasibility of a methodology utilising gentle enzymatic lysis of cells containing internalised particles and direct analysis of the lysates for the particle size, agglomeration state and concentration, is investigated. It is demonstrated that following internalisation, all types of studied silica particles partially agglomerate/aggregate, with the degree and rate of the observed transformation closely correlated with the initial particle surface chemistry. Several different particle populations are noted and characterised in terms of their size and concentration. Good agreement between different complementary techniques is reached in terms of the average particle diameter. Particle concentration is determined here with techniques capable of mass and number-based measurements, with limitations of approaches utilising signal conversion to equivalent particle numbers identified and discussed.

Received 5th December 2017,
Accepted 22nd January 2018

DOI: 10.1039/c7tx00323d

rsc.li/toxicology-research

Introduction

Nanomaterials are increasingly being used to overcome many scientific, economic and industrial challenges, with silica (SiO_2) nanoparticles (NP) being one of the most commonly produced.[1] Due to their anti-caking properties, SiO_2 NP have found application in food production,[2] and they are also used in paints and coatings,[3] microelectronic devices,[4] as well as imaging probes in biomedical sectors.[5,6] Such a widespread use of nanomaterials (NM) has raised safety concerns, arising from a possibility of their uncontrolled release from the commercial product and subsequent impact on humans and the environment.[7] Once ingested, inhaled or absorbed through the skin, NP can interact with individual cells within the body and trigger various biological and toxicological responses.[8,9] This typically occurs following particle internalisation by the cells. Internalised particles undergo complex structural and functional changes induced by their intracellular processing.[8,10] Therefore, in order to understand the impact of NP and link the type of transformation they undergo with the effect it has on cells, their properties following internalisation by the cells need to be thoroughly characterised.

There are several key particle characteristics that should be studied. According to the European Commission definition of NM, particle size, agglomeration and aggregation state, as well as concentration must all be considered.[11] It is also important to note that for the purposes of toxicological screens, NM concentration expressed in particle number terms, rather than mass fraction has been identified as a more relevant metric.[12,13]

Despite these requirements, only recently have methods for reliable particle characterisation in complex biological matrices started to emerge. For example, single particle inductively coupled plasma mass spectrometry (spICP-MS) has been shown as a promising tool for the characterisation of silver NP accumulated in a tissue.[14] spICP-MS while being very useful in characterisation of metal and metal oxide based NP, struggles with elements with poor ionisation and high signal contribution of procedural blanks, such as silicon.[15] As an alternative, a method based on the particle tracking analysis (PTA) platform coupled on-line to the asymmetric flow field-flow fractionation (AF4) system using ICP-MS and multi-angle light scattering (MALS) detection has recently been developed and its potential for size and number-based SiO_2 NP characterisation in the presence of high concentrations of biological serum has been demonstrated.[16]

[a]*LGC Limited, Queens Road, TW11 0LY Teddington, UK.*
E-mail: dorota.bartczak@lgcgroup.com
[b]*Physikalisch-Technische Bundesanstalt, Abbestraße 2-12, D-10587 Berlin, Germany*

†Electronic supplementary information (ESI) available: Size and zeta-potential analysis of NP water suspensions, size analysis of the NP core, total and post-channel Si quantification and Si mass conversion to particle number, EDAX and SAXS analysis of internalised particles. See DOI: 10.1039/c7tx00323d

Here we show for the first time that AF4/MALS/ICP-MS in conjunction with PTA can also be applied for the characterisation of particles internalised by mammalian cells. The evolution of particle characteristics upon internalisation by cells was studied using the HepG2 cell line derived from the human liver as a model system, since the liver is a common target organ following particle ingestion, inhalation or absorption through skin.[17] Two types of silica particles, well-characterised under the EMRP NanoChOp project,[18] were chosen for this study, since silica is one of the most popular types of commercially used nanomaterials worldwide and produced in high volumes.[1] These particles were similar in size and differed only in surface chemistry. However, since surface chemistry has been shown before to greatly affect the cell behaviour upon exposure to NM,[8,10,19,20] this is an important parameter to study. The aim was to investigate the uptake of silica particles by cells and any possible changes in particle properties due to processing by the cell machinery.

The particle size and agglomeration state were determined by AF4/MALS and PTA whilst more traditional techniques, like transmission electron microscopy (TEM) and small angle X-ray scattering (SAXS), were used to provide confirmatory qualitative measurements of the agglomerates. The content of particles in the individual size fractions, representative of primary and agglomerated/aggregated particles, was determined by PTA in number-based terms and by AF4/ICP-MS as a mass fraction of silicon. The mass fraction of silicon was then converted to particle numbers in order to allow a comparison between the techniques. The limitation of such an approach is discussed here. Moreover, the influence of particle agglomeration/aggregation on particle number measurements, as well as problems associated with using the AF4/ICP-MS approach to silicon content quantification in such complex samples are also debated.

Results and discussion

Particle internalisation by cells

The first steps in our study were to confirm that both types of NM are indeed internalised by the cells and to quantify their internalisation rate. Representative TEM images, shown in Fig. 1, taken after 24 h exposure of the cells to the particles, clearly demonstrate the presence of particles inside the cells. As indicated by the red arrows, the particles are locked inside the intracellular organelles, since they are surrounded by a double membrane. Additionally, EDAX analyses (Fig. S1, ESI†) confirm that the imaged particles were composed of silica. The amount of particles internalised by the cells following 24 h exposure was determined using ICP-MS (see section S2, ESI†) and presented as a mass-fraction of silicon or as a percentage of total introduced silicon in cell media (Table 1). It was found that aminated silica was taken up by the cells at higher rates than plain silica, with nearly 20% of the introduced amount of silicon present inside the cells. Differences seen in the uptake rates (more than 5% of the total introduced silicon) could be attributed to the differences in the surface chemistry of the two materials and their zeta-potential (section S3, ESI†), since their sizes are similar (section S4, ESI†). As opposed to close-to-neutral aminated silica, plain particles show a strong negative charge and therefore could potentially be repelled from a negatively charged cellular membrane, resulting in the observed lower internalisation rates.

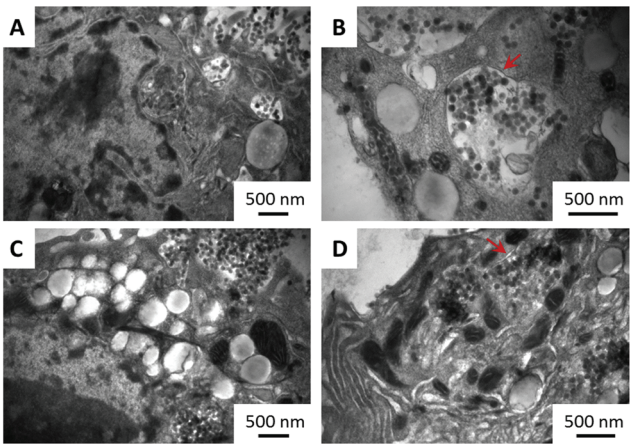

Fig. 1 Representative TEM images of plain (A and B) and aminated (C and D) silica particles internalised by HepG2 cells (A and C) or locked in intracellular organelles (B and D) following 24 h incubation. Arrows indicate the double membrane surrounding organelles. Scale bars are 500 nm.

Table 1 Quantification of the internalisation rate of silica particles by ICP-MS (average ± std dev; n = 3)

	NP internalisation rate	
Material	mg kg^{-1} of Si in 8×10^6 cells per ml	% of introduced
Plain silica	258 ± 72	12 ± 2
Aminated silica	392 ± 62	17 ± 2

Prior to sizing and quantification, internalised particles were released from the cells and cell organelles with commercially available cell lysis buffer. To ensure that the potential changes in particle characteristics are a true effect of their uptake and incubation in cell lysis buffer, spiked analogues were also studied alongside. Spiked samples were prepared by mixing a fresh portion of plain and aminated particles with cell lysis buffer containing already lysed (particle-free) cells and keeping the mixture under the same conditions and for the same duration of time as the samples containing internalised particles. The amount of particles and the number of cells in the spiked samples were maintained the same as those in the internalised samples, to avoid any potential concentration-induced effects.

Qualitative examination of the internalised particles

Both, spiked and internalised samples were examined qualitatively by TEM and SAXS, for potential changes in the shape

and/or agglomeration/aggregation state. Representative TEM images are shown in Fig. 2. There are clear differences between the spiked and internalised samples, with particle agglomeration and aggregation seen in the images of internalised particles, as indicated by red arrows. In the case of aminated particles (image F) in addition to agglomerates, aggregated and primary particles a minor population of smaller objects of similar contrast is also seen, which could be representative of a smaller particle fraction present in the starting material. Differences between the plain and aminated particles are also seen in the images of spiked samples, with the plain particles appearing mostly as individual (dispersed) primary spherical particles, whilst aminated silica are more irregular in shape. These agree well with the SAXS results, as displayed in Fig. 3, where the experimental data shown are superimposed with fits of a model function for solid spherical particles with a Gaussian size distribution. Only in the case of the spiked plain silica particles, this model can describe the full measured range of q. For the other samples, deviations appear mainly in the Guinier region (where $q < 0.1$ nm^{-1}), whereas the position of the minima for $q > 0.1$ nm^{-1} does not change. This indicates the agglomeration/aggregation of the particles, with a similar size of primary particles within those agglomerates/aggregates. The core size, extracted from the model fitting, agrees with the data obtained for the particles suspended in water as shown in section S5,† as well as the TEM images. SAXS data, in agreement with TEM, suggest that only plain particles remain stable in contact with lysed cells, whilst aminated silica aggregates/agglomerates. Processing using the cells leads to agglomeration/aggregation in both cases, which is also evident from the TEM images.

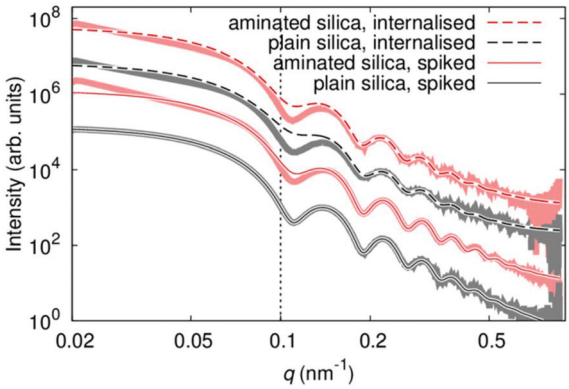

Fig. 3 SAXS scattering curves for plain (red) and aminated (black) silica particles spiked into lysed HepG2 cells (solid lines) or after being internalised by HepG2 cells, then lysed (dashed lines). The experimental data are represented by the thick lines, while the thin lines correspond to simulations of non-agglomerated particles. The dotted line represents the upper limit of the Guinier region.

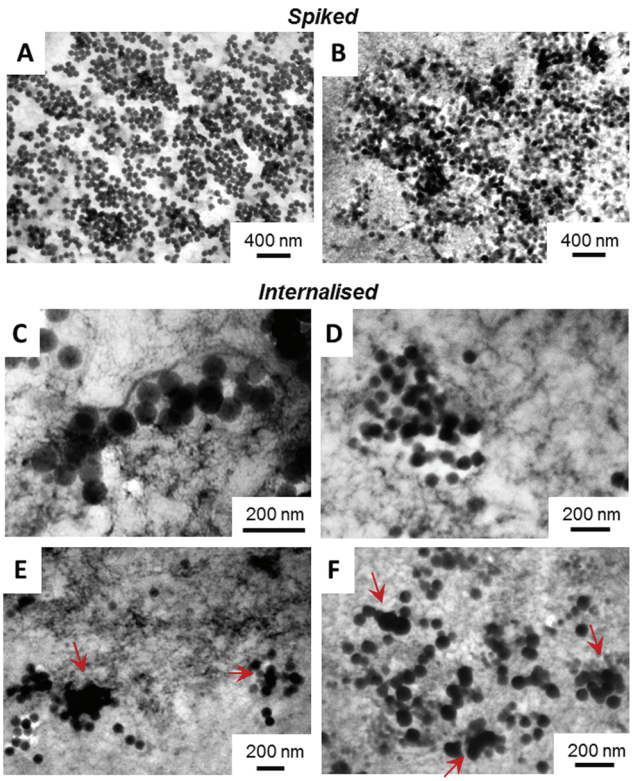

Fig. 2 Representative TEM images of plain (A, C and E) and aminated (B, D and F) silica particles spiked into lysed HepG2 cells (A and B) or after being internalised by HepG2 cells, then lysed (C–F). Arrows indicate aggregated/fused particles. Scale bars as shown in the images.

Particle size measurements

Size analyses of plain and aminated silica, in terms of their hydrodynamic diameter, were performed using an on-line AF4/MALS and using PTA. Typical fractograms of fractions separated using AF4 and detected using MALS are shown in Fig. 4. Prominent differences between the spiked and internalised samples, as well as between the plain and aminated particles are seen. For spiked samples, plain particles appear as one distinctive fraction peak, eluting at about 28 min, whilst the majority of aminated silica particles elute much later, at around 38 min, suggesting that the structural changes seen in TEM micrographs are correlated with their increased retention time in the AF4 channel. In contrast, the fractograms of both, plain and aminated internalised particles show two distinctive fraction peaks eluting at around 31 and 35–36 min. The smaller peak appearing in the fractograms of aminated particles at an elution time of 18–25 min could be attributed to a fraction of smaller particles, also seen in the TEM images. Common between all fractograms, a sharp peak at around 5 min elution time, is a typical, so called 'void peak', representing particles not retained during the focusing step and/or larger objects eluted in a steric mode.[21] The summary of particle size values determined by MALS is shown in Table 2. The diameter of plain silica particles spiked into the lysates increased compared to particle water suspensions (section S4†), which could be attributed to the formation of an organic corona, since the particles appeared on the TEM images (Fig. 2), as mostly primary spheres of about 80 nm size (and only inorganic components can be detected by TEM). The size

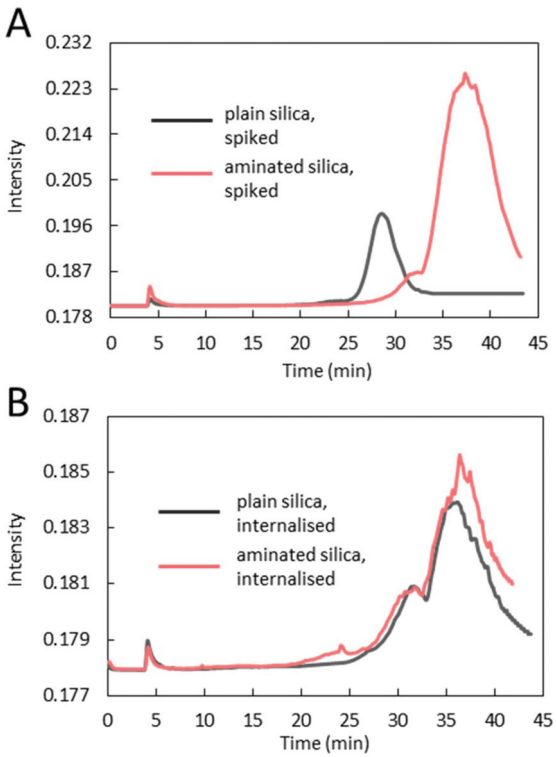

Fig. 4 Representative AF4/MALS fractograms of plain and aminated silica particles spiked into lysed HepG2 cells (A) or after being internalised by HepG2 cells, then lysed (B).

Table 2 AF4/MALS size analysis of spiked and internalised silica particles (average ± std dev; n = 4)

	Particle diameter (nm)			
		Internalised and processed by cells		
Material	Spiked into lysates	Fraction 1	Fraction 2	Fraction 3
Plain silica	94 ± 4	n/a	110 ± 5	226 ± 14
Aminated silica	135 ± 47	38 ± 1	134 ± 10	254 ± 12

of spiked aminated silica measured at the top of the peak eluting at 35–36 min increased by around 40 nm more than the size of plain particles, which suggests some additional structural changes, such as agglomeration or aggregation in addition to the formation of a thicker organic corona. In the case of internalised aminated particles three distinctive size fractions were found. The smallest in size, fraction 1 (around 38 nm) is most likely representative of less abundant smaller particles. A similar size fraction was not detected in a sample of internalised plain particles. The average size of the particles in fraction 2, seen for both materials, was around 110 nm for plain and 134 nm for aminated silica. This suggests a slightly higher degree of change to aminated particles occurring after internalisation by cells. Size fraction 3, attributed to aggregates and/or agglomerates of higher order, was again slightly larger for aminated particles than plain particles.

Spiked and internalised particles were also characterised with an alternative technique (PTA) to provide confirmatory and complementary measurements on the size of the detected fractions. Spiked and internalised samples were diluted around 20× in 5 ml Tris-HCl pH 7.4 buffer (also used as a carrier for AF4/MALS/ICP-MS) to minimise the matrix (lysed cells) effects on the measurement and to match the composition of the AF4 eluate. This dilution was found optimal for the measurement of internalised samples. Representative PTA size distribution graphs are shown in Fig. 5, whilst the average size values obtained for the three main fractions are summarised in Table 3. Similar to AF4/MALS, PTA measurements indicate that the spiked plain particles are predominantly monomodal, whilst particles that went through the cell machinery consist of multiple size fractions. The diameter of the spiked particle samples agrees well with the values obtained using AF4/MALS, despite the differences in the physical basis of the

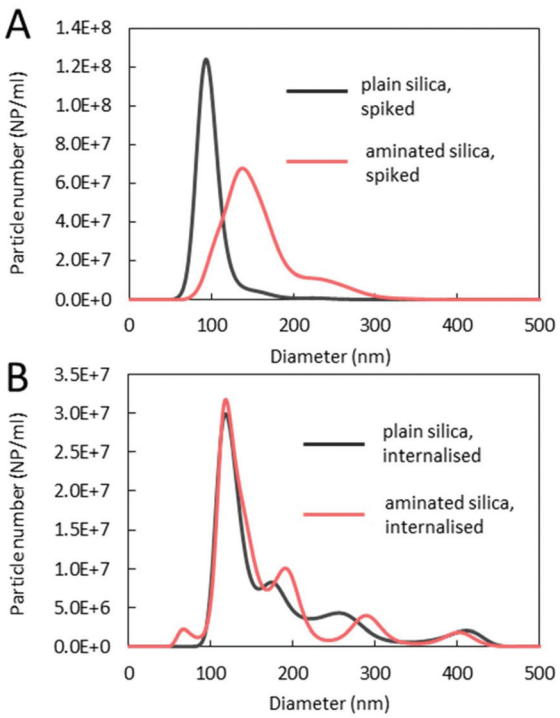

Fig. 5 Representative PTA size distribution graphs of plain and aminated silica particles spiked into lysed HepG2 cells (A) or after being internalised by HepG2 cells, then lysed (B).

Table 3 PTA size analysis of spiked and internalised silica particles (average ± std dev; n = 4)

	Particle diameter (nm)			
		Internalised and processed by cells		
Material	Spiked into lysates	Fraction 1	Fraction 2	Fraction 3
Plain silica	93 ± 2	n/a	113 ± 6	255 ± 6
Aminated silica	138 ± 6	57 ± 7	122 ± 5	272 ± 14

measurements, with PTA reflecting particle movement (velocity) under the Brownian motion,[22] while MALS is a scattering intensity based technique.[23] A larger modal diameter of aminated particles than plain particles spiked into the lysates along with a much broader size distribution seen in PTA graphs indicates that the organic layer acquired from the media might not be uniform in size whilst the presence of small agglomerates/aggregates cannot be excluded. The shoulder on the right hand side is most likely representative of higher order agglomerates/aggregates. Differences between the plain aminated silica spiked into the lysates are attributed to the original surface functionality with near-neutral charge of aminated particles likely affecting their stability. Similarly to AF4/MALS, PTA's fraction 1, representative of less abundant smaller particles, was only detected in an internalised aminated silica sample. The average size values of particles within that fraction were larger than the diameter measured using AF4/MALS, which could be explained by the size detection limit of PTA, which for silica particles is in the range of 40–50 nm with our experimental set-up (detailed in the Experimental section). Fraction 2 detected by PTA in the aminated and plain internalised samples is similar in size to fraction 2 detected by AF4/MALS within associated measurement errors, suggesting the presence of particles with a thick organic shell, since the modal diameter of particles in this size fraction is too small to represent small agglomerates/aggregates only and too narrow to suggest a mixture of monomers and small agglomerates/aggregates. Fraction 3 detected using PTA is a representative of agglomerates and aggregates with average diameter also in close agreement with AF4/MALS data. In addition to the three main fractions, PTA also detected two more fractions within the agglomerated/aggregated particle population: (161 ± 10) nm and (405 ± 11) nm for plain silica or (185 ± 6) nm and (411 ± 12) nm for aminated silica, suggesting much better resolution of this technique. It is also important to note that PTA graphs provide information about a relative content of the detected fractions, since PTA is a number-based technique. In contrast AF4/MALS is an intensity-based technique and therefore the relative heights of size fractions cannot be directly related to content. According to the PTA graphs, fraction 2 is the most populated out of all size fractions.

Particle concentration determination

With MALS being an intensity-based technique, particle content in the samples was measured with the ICP-MS detector, as a mass fraction of silicon. The position (*i.e.* elution time) and the number of the peaks shown in the representative AF4/ICP-MS fractograms in Fig. 6 are the same as those on the AF4/MALS fractograms, but the relative height between the peaks is different. This is, due to highlighted before, principle of detection. MALS measures the analyte scattering intensity, which is higher for larger objects, while ICP-MS measures the mass-content of silicon in the peaks and offers information on the quantitative relationship between the fractions. The summary of the total mass-fraction of particulate silicon

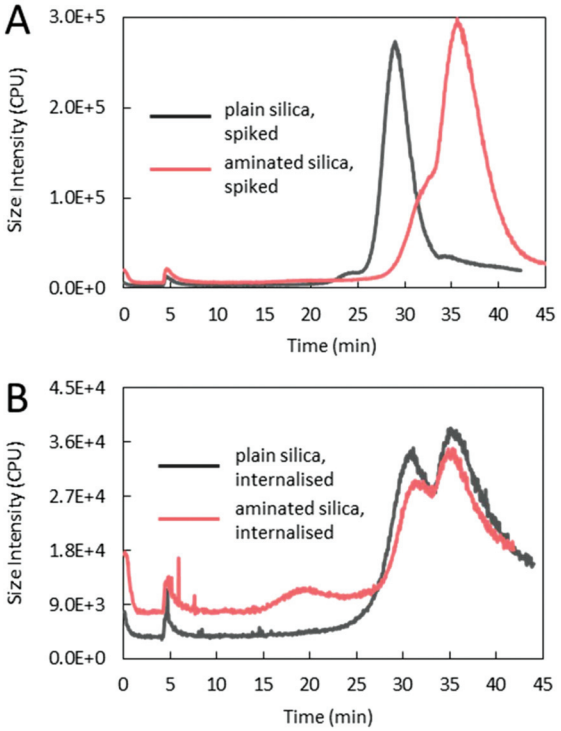

Fig. 6 Representative AF4/ICP-MS fractograms of plain and aminated silica particles spiked into lysed HepG2 cells (A) or after being internalised by HepG2 cells, then lysed (B).

measured in the samples is shown in Table 4, whilst the break-down for individual size fractions is shown in Table S7D.† More silicon was detected in the spiked aminated samples than in the spiked plain samples, nevertheless for both materials, the quantified element content was lower than expected. For plain particles this equated to over 85% recovery rate from the expected value (based on Si content values of (257.6 ± 72.0) μg g^{-1} for the expected content and (219.4 ± 8.9) μg g^{-1} for the measured content, as shown in Table 4), whilst for aminated particles, only to about 64% (number derived in the same way as that for plain material), as summarised in Table S7E.† The lower than expected recovery rate of particles can be attributed to a loss in the AF4 system, *e.g.* sticking of the particles to the AF4 membrane induced by the cross-flow during sample separation and/or sample dissolution, as previously reported.[16] This is supported by the analysis without application of the cross-flow, with (99.6 ± 1.8)% of silicon recovered for the plain material. In the case of the aminated material only (71.0 ± 3.0)% of silicon was accounted for, suggesting particle destabilisation and/or sticking to PEEK tubing, which is expected for particles showing near-neutral net charge (section S3†). Also, for the internalised material, a higher silicon content and a recovery rate (total in all fractions of almost 30%) were observed for plain silica than for aminated silica (total recovery of only around 11.6%), with overall much lower recovery rates found for both materials, compared to the spiked samples. This could be explained by an increased

Table 4 Measured with AF4/ICP-MS sum of particulate silicon mass-fraction and equivalent number of particles (average ± std dev, n = 4)

Material	Expected Si content (μg g^{-1})	Measured particulate silicon content (μg g^{-1})[a]		Equivalent particle number (NP g^{-1})[b]	
		Spiked into lysates	Internalised and processed by cells	Spiked into lysates	Internalised and processed by cells
Plain silica	258 ± 72	219 ± 9	75 ± 3	(8.2 ± 0.3) × 10^{11}	(3.0 ± 0.1) × 10^{10}
Aminated silica	392 ± 62	253 ± 8	45 ± 1	(6.3 ± 0.2) × 10^{11}	(3.6 ± 0.2) × 10^{11}

[a] As sum of all detected fractions; breakdown to individual size-fractions is shown in Table S7D. [b] Assuming diameter of internalised fractions based on MALS measurements.

destabilisation, including aggregation induced by the intracellular processing of silica and/or potential loss during the lysate preparation. Interestingly, for both materials, the highest content of silicon was found in fraction 3, representative of agglomerates/aggregates, whilst the lowest content was found in fraction 1, representative of smaller particles (for aminated material, for which this size fraction was detected). However, when a mass fraction of silicon was converted to particle numbers, as explained in sections S6 and S7,† this trend was reversed with the lowest number of particles present in the agglomerate/aggregate fraction. Differences between expressing the particle content in mass and number based terms are of particular importance in the assessment of their impact on bio-systems and in the design of experiments for nanotoxicology, where the appropriate dosimetry is crucial, as highlighted by other research groups.[13]

The particle number in the samples was also measured using PTA and the obtained values were compared to the expected particle content, shown as particle recovery rates in Table 5 and Table S8.† The amount of particles measured in a sample of spiked plain silica was in agreement with the expected number of particles. In contrast only around 68% out of the total expected number of aminated silica were found in the sample. Almost 30% loss of aminated silica compared to plain silica could be explained by particle destabilisation, due to near-neutral net charge agglomeration/aggregation (since the expected particle number is based on monomers) and/or sticking to the tubing and top plate. Nonetheless, the obtained numbers are in agreement with the recovery rates obtained using the AF4 based system with no cross-flow (as quoted in a previous paragraph). Analyses of the fractions detected in the internalised plain silica samples (Table S8†) have shown a higher number of particles in fraction 2 than in fractions representing agglomerates/aggregates, similar to AF4 results. This was not the case for the aminated material, where the sum of particles in fractions representing agglomerates was not significantly different from the number of particles in fraction 2. It is possible that agglomerated/aggregated particles interact stronger with the AF4 membrane during the separation step than particles in fraction 2, leading to a higher loss in the system. Another explanation could be a systematic error made during silicon mass-fraction conversion to particle number terms. Such a conversion assumes spherical geometry of particles, whilst aggregates/agglomerates are not spheres. Also the diameter of the particles in AF4/ICP-MS fraction 3 is an approximated average between the dimers, trimers and tetramers. In fact only for spiked plain silica, which were found to be mostly monodisperse and spherical, the number measured with PTA and equivalent number calculated based on the AF4/ICP-MS measurements are in agreement (when sample loss in the channel is accounted for). This illustrates that the conversion of the elemental mass fraction to particle terms is reliable only for the particles of known and well-defined geometry, precisely known size and with a narrow size distribution rather than polydispersed. Relatively low number of particles in fraction 1 of aminated silica measured with PTA, in comparison with AF4/ICP-MS, could be explained, as mentioned before, by a lower detection limit of PTA (40–45 nm), meaning that smaller particles are simply not counted, as opposed to AF4/ICP-MS detection which was shown to be accurate even for silica particles as small as 20 nm.[24] Overall material recovery rates based on PTA measurements were higher than the values obtained using AF4/ICP-MS which, as already mentioned, is associated with the instrumental loss of the material during AF4 separation (*i.e.* cross-flow induced sticking to the AF4 membrane). Nonetheless, even with PTA only just over 40% of plain and 25% of aminated material were counted. The lower than

Table 5 Particle number and recovery rates from expected particle number determined by PTA (average ± std dev, n = 4)

Material	Spiked into lysates		Internalised and processed by cells	
	Measured particle number (NP g^{-1})	Recovery rate[a] (%)	Measured particle number (NP g^{-1})	Recovery rate[a] (%)
Plain silica	(10.2 ± 0.4) × 10^{11}	98.9 ± 4.0	(4.4 ± 0.1) × 10^{11}	42.3 ± 0.9
Aminated silica	(10.7 ± 0.3) × 10^{11}	68.1 ± 2.0	(4.1 ± 0.1) × 10^{11}	26.8 ± 0.8

[a] From the expected particle concentration (plain 10.3 × 10^{11} NP g^{-1}; aminated 15.7 × 10^{11} NP g^{-1}).

expected particle counts could be attributed to a combination of factors, such as agglomeration/aggregation (since the expected particle number is based on monomers), dissolution as well as loss during the lysate preparation. A further decrease in the recovery rate seen for aminated silica compared to plain silica is most likely associated with already emphasised lower stability of these particles.

Experimental

NP internalisation

HepG2 cells (passage 80–83, LGC Standards) were seeded in a culture dish (6-well microplate, PAA Laboratories) at a density of 100 000 cells per cm^2. The cells were grown in 2.5 ml EMEM media (Sigma-Aldrich) supplemented with 10% FBS (PAA Laboratories) for 24 h in an air balanced incubator at 5% CO_2, 37 °C. After the initial 24 h incubation, cell culture media were removed and freshly prepared plain and aminated silica NP suspensions were introduced (2.5 ml per well, 500 μg g^{-1} in 10% FBS EMEM). The cells were incubated for a further 24 h, washed twice with PBS (2.5 ml per well, Sigma-Aldrich) and harvested with accutase solution (0.6 ml per well, Sigma-Aldrich) until detached. Collected cell suspensions were either mineralised using acid supported microwave digestion (Milestone, Analytix) and analysed for the total content of ^{28}Si using ICP-MS (7700×, Agilent Technologies) operating in a hydrogen mode (see section S2† for more details) or processed prior to TEM imaging. In detail, the cell suspension was transferred to a 1.5 ml plastic tube and centrifuged (450*g*, 5 min, 4 °C). The supernatant was decanted and the cell pellet was redispersed in a glutaraldehyde (3%, Agar Scientific)/formaldehyde (4%, Agar Scientific) mixture in piperazine-1,4-bis-2-ethanesulfonic acid buffer (PIPES, 0.1 M, pH 7.2; Sigma-Aldrich) and incubated for 15 min at room temperature. The cells were centrifuged (450*g*, 5 min, 4 °C) and decanted. A drop of sodium alginate (5%, in water, Sigma Aldrich) was added to the cell pellet, followed by a 1 : 1 mixture of PIPES (0.5 ml, 0.2 M) and calcium chloride solution (0.5 ml, 0.2 M in water, Sigma Aldrich). After 15 min, when the alginate settled, the supernatant was removed gently and the embedded cell pellet was transferred into a glass vial and fixed with osmium tetroxide (1%, 0.1 M PIPES; Agar Scientific) for 1 h. The fixed pellet was washed twice with water and stained with uranyl acetate (2%, in water, Agar Scientific) for 20 min. The pellet was then dehydrated in 30%, 50%, 70%, and 95% ethanol solutions, 10 min each, and then in absolute ethanol over 20 min, twice. The dehydrated pellet was washed with acetonitrile and then incubated overnight in a 1 : 1 mixture of acetonitrile and TAAB resin (Agar Scientific) and finally embedded in TAAB resin followed by polymerisation at 60 °C for 24 h. Resin blocks were cut with a Leica RM 2255 microtome to obtain ultrathin sections (90–100 nm thickness). The sections were deposited on TEM grids and stained with Reynolds lead stain (Sigma-Aldrich) prior to imaging with an FEI Tecnai-12 TEM operating at 80 kV bias voltage and equipped with a TEAM™ EDS Apollo XLT X-ray microanalysis platform (Biomedical Imaging Unit, Southampton, UK).

Release of internalised NP

HepG2 cells were seeded in a culture dish (T175, Corning, Fisher Scientific, UK) at a density of 100 000 cells per cm^2. The cells were grown in 25 ml EMEM media supplemented with 10% FBS for 24 h in an air balanced incubator at 5% CO_2, 37 °C. After the initial 24 h incubation, cell culture media were removed and freshly prepared plain and aminated silica NP suspensions were introduced (25 ml per flask, 500 μg g^{-1} in 10% FBS EMEM). The cells were incubated for a further 24 h, washed twice with PBS (5 ml per flask) and harvested with accutase solution (5 ml per flask) until detached. The detached cells were transferred into a 50 ml plastic centrifuge tube, along with 5 ml of cell culture media and counted with an automated cell counter (Vi-CELL XR, Beckman Coulter, Inc.). The cell suspension was then centrifuged (450*g*, 5 min, 4 °C), the supernatant was removed and the cell pellet was washed once with DPBS (5 ml, Sigma-Aldrich) and resuspended in CelLytic M reagent (125 μl per 1 000 000 cells; Sigma-Aldrich). The cells were lysed for 15 min at room temperature on a shaker, and then stored at 4 °C prior to analysis using AF4/MALS/ICP-MS and PTA (within 24 h). Samples for TEM were centrifuged (20 000*g*, 15 min, 4 °C), then processed and imaged as described in the previous paragraph.

Cell lysate spiking with NP

HepG2 cells grown for 24 h and harvested under the same conditions as described in the previous paragraph were transferred into a 50 ml plastic centrifuge tube, along with 5 ml of cell culture media and counted with an automated cell counter (Vi-CELL XR, Beckman Coulter, Inc.). Cell suspension was then centrifuged (450*g*, 5 min, 4 °C), supernatant was removed and the cell pellet was washed once with DPBS (5 ml, Sigma-Aldrich) and resuspended in a CelLytic M reagent (125 μl per 1 000 000 cells; Sigma-Aldrich). The cells were lysed for 15 min at room temperature on a shaker, and then stored at −80 °C prior to spiking with plain and silica NP. Prior to spiking the cell pellet was thawed and warmed up to room temperature, and then mixed with plain and aminated NP to a final concentration of ∼257.6 or ∼391.8 μg ml^{-1} of silicon per 8 000 000 cells (over 200-fold dilution), respectively to match the amount of silicon present in the internalised lysates. Spiked samples were then incubated for 15 min at room temperature on a shaker and stored at 4 °C prior to analysis using AF4/MALS/ICP-MS and PTA (within 24 h). Samples for TEM were centrifuged (20 000*g*, 15 min, 4 °C), then processed and imaged as described in the 'NP internalisation' paragraph.

Sizing and quantification of internalised NP with AF4/MALS/ICP-MS

Measurements were performed with an AF4 system (AF2000, Postnova Analytics) hyphenated to MALS (PN3621, Postnova Analytics), UV (Accela PDA, Thermo Electron) and ICP-MS (7700×, Agilent Technologies) detectors. AF4 was fitted with an

analytical ceramic frit separation channel, while ICP-MS was equipped with a μmist nebuliser, wide torch and Scott spray chamber. The instrument performance was monitored in-house on day-to-day basis against a standard tune solution (Agilent Technologies). MALS and UV detectors were calibrated with bovine serum albumin (Sigma-Aldrich) with the angles normalised to a polysulfonate particle standard (Z-POS-PSS67k, Postnova Analytics). The instrument was switched on at least 30 min before the measurements, with the AF4 channel temperature set and maintained at 25 °C throughout the measurements. Cell lysates and spiked samples were diluted 10-fold gravimetrically with 5 mM Tris-HCl pH 7.4 buffer (Sigma-Aldrich) before injecting into the system using calibrated 12.8 μl loop. Separation was performed with a 10 kDa regenerated cellulose membrane (Postnova Analytics), 5 mM Tris-HCl pH 7.4 carrier and a method with a decay field (cross-flow = 2 ml min^{-1} for 5 min, then cross-flow = 2 → 0.5 ml min^{-1} linear decay for 10 min, followed by cross-flow = 0.5 → 0 ml min^{-1} power 7 decay for 14 min and finally cross-flow = 0 ml min^{-1} for 12 min). The injection time was 3 min. After every three injections the system was purged with 12.5 mM Tris-HCl pH 7.4 followed by the carrier, whilst the AF4 instrument was cleaned with 10% methanol at the end of each day. ICP-MS was operated in hydrogen gas mode, monitoring Si at m/z 28 and 29 (Ge at m/z 72 was used as the internal standard). External calibration was performed with NIST SRM 3150 (elemental Si), using the post-channel quantification approach developed by V. Nischwitz *et al.*[25] The results shown in section S7† are the average of n = 4 measurements with the corresponding standard deviation. The size of the particles was determined with a MALS detector directly using 17 out of the 21 available angles and a sphere model fit. The equivalent particle number was calculated from the weight of NP (assuming density of around 2 g cm^{-3} and the diameter was determined with sizing detectors, see section S7† for more details).

Sizing of internalised NP using PTA.

Measurements and analysis of the recorded movies were performed by PTA (NS500, Malvern Instruments Ltd) equipped with a light source (violet diode laser, 405 nm, power <60 mW), electron multiplying charge coupled device (EMCCD) camera and PTA 3.0 software. The instrument was switched on at least 30 min before the measurements. Before loading the sample, the gasket was cleaned with 0.1 μm filtered 10% MicroSol (Anachem), whilst the top plate and prism holder were cleaned with 0.1 μm filtered 10% Microsol followed by 0.1 μm filtered 70% ethanol (Sigma-Aldrich) in water. All parts were rinsed with 0.1 μm filtered ultrapure water (18.2 MΩ cm at 25 °C) and dried with compressed air. The temperature was set and maintained at 25 °C throughout the measurements. Movies were recorded over 160 s, with 30 s equilibration time prior to each measurement. Camera levels were set to 9. No filters were used. The performance of the instrument was checked daily with gold particles (NIST RM 8013, nominal diameter 60 nm) diluted ~50 times with ultrapure filtered water (18.2 MΩ cm at 25 °C). The following parameters were fixed: viscosity was set to 0.8905 mPa s, detection threshold was set to 5 for spiked samples and 3 for the internalised samples, whilst other parameters were set to automatic. A minimum of 2000 completed tracks were recorded per measurement. The obtained data were collated and further processed using Excel 2010. The values shown are the average of n = 4 measurements with the corresponding standard deviation.

Sizing of internalised NP with SAXS

The SAXS experiments were performed at the four-crystal monochromator beam line of PTB at the synchrotron radiation facility BESSY II.[26] The samples were filled into disposable borosilicate glass capillaries with an inner diameter of 1 mm and a wall thickness of 10 μm and enclosed by welding. The synchrotron radiation with a photon energy of (6000 ± 0.6) eV was collimated using pinholes to a size smaller than 0.5 × 0.5 mm^2 and focused on the sample. The incident photon flux was measured using a transparent photodiode located in front of the sample before the guard pinhole. A removable, calibrated diode behind the sample was used to measure the transmittance of the sample. The scattered radiation was collected by using an in-vacuum PILATUS 1 M detector with a pixel size of (172.1 ± 0.2) μm at a distance of (4574.8 ± 0.5) mm behind the sample.[26] The pure cell lysate was measured in addition to the samples as a blank. The resulting scattering images were treated in the standard way[27] by averaging azimuthally about the beam centre and normalizing to the incident beam intensity and transmittance of the samples, and finally the subtraction of the blank and converting into momentum transfer q.

Conclusions

Methodology based on the combination of AF4/MALS/ICP-MS and PTA (supported by TEM and SAXS) was used to demonstrate that silica particles undergo complex physicochemical changes once internalised by cells. These changes are actively induced by the intracellular processing machinery, since they did not occur upon incubation with deactivated (lysed) cells under analogous conditions. It was found that the initial surface chemistry of particles also plays a role, influencing the degree, type and relative ratio of transformation. The particles were found to partially agglomerate/aggregate as well as to undergo other changes, like adsorption of organic corona. Several different size fractions were found and the average diameter of objects within these fractions, measured using PTA and AF4/MALS, was in good agreement. However, the quantification of the amount of material in the individual fractions proved to be more challenging. Measurements of the silicon mass fraction using AF4/ICP-MS were affected by the sample loss in the AF4 system during separation, whilst the particle numbers determined by PTA were influenced by sample agglomeration/aggregation. To enable data comparison

between the techniques, mass fraction of silicon was converted to particle number terms, but such an approach was only found successful for particles of well-defined (*i.e.* spherical) geometry and low polydispersity. The methodology shown here is applicable to other types of inorganic materials and since understanding the particle changes upon internalisation by cells is essential in the assessment of their biological and toxicological impact, it is expected to be of wide interest.

Conflicts of interest

There are no conflicts of interest to declare.

Acknowledgements

This work was supported by the European Metrology Research Programme. We thank G. Roebben and V. Kestens from the JRC for providing base silica material and ampouling the aminated silica and Z. Varga from Hungarian Academy of Sciences for the preparation of the aminated material. Biomedical Imaging Unit, Southampton, UK is gratefully acknowledged for the technical support with TEM/EDAX analysis.

Notes and references

1 F. Piccinno, F. Gottschalk, S. Seeger and B. Nowack, Industrial production quantities and uses of ten engineered nanomaterials in Europe and the world, *J. Nanopart. Res.*, 2012, **14**, 1109.
2 H. Bouwmeester, P. Brandhoff, H. J. P. Marvin, S. Weigel and R. J. B. Peters, State of the safety assessment and current use of nanomaterials in food and food production, *Trends Food Sci. Technol.*, 2014, **40**, 200.
3 A. Al-Kattan, A. Wichser, R. Vonbank, S. Brunner, A. Ulrich, S. Zuin, Y. Arroyo, L. Golanski and B. Nowack, Characterization of materials released into water from paint containing nano-SiO2, *Chemosphere*, 2015, **119**, 1314.
4 A. I. Kingon, J. P. Maria and S. K. Streiffer, Alternative dielectrics to silicon dioxide for memory and logic devices, *Nature*, 2000, **406**, 1032.
5 G. Iovino, M. A. Malvindi, S. Agnello, G. Buscarino, A. Alessi, P. P. Pompa and F. M. Gelardi, Optical and morphological properties of infrared emitting functionalized silica nanoparticles, *Mater. Chem. Phys.*, 2013, **14**, 763–769.
6 R. Kumar, I. Roy, T. Y. Ohulchanskyy, L. N. Goswami, A. C. Bonoiu, E. J. Bergey, K. M. Tramposch, A. Maitra and P. N. Prasad, Covalently dye-linked, surface-controlled, and bioconjugated organically modified silica nanoparticles as targeted probes for optical imaging, *ACS Nano*, 2008, **2**, 449–456.
7 M. R. Wiesner, G. V. Lowry, P. Alvarez, D. Dionysiou and P. Biswas, Assessing the risks of manufactured nanomaterials, *Environ. Sci. Technol.*, 2006, **40**, 4336.
8 A. E. Nel, L. Madler, D. Velegol, T. Xia, E. M. V. Hoek, P. Somasundaran, F. Klaessig, V. Castranova and M. Thompson, Understanding biophysicochemical interactions at the nano–bio interface, *Nat. Mater.*, 2009, **8**, 543.
9 A. Lesniak, F. Fenaroli, M. P. Monopoli, C. Åberg, K. A. Dawson and A. Salvati, Effects of the Presence or Absence of a Protein Corona on Silica Nanoparticle Uptake and Impact on Cells, *ACS Nano*, 2012, **6**, 5845.
10 D. Bartczak, M. O. Baradez, H. Goenaga-Infante and D. Marshall, Label-free monitoring of the nanoparticle surface modification effects on cellular uptake, trafficking and toxicity, *Toxicol. Res.*, 2015, **4**, 169.
11 EC, *Commission Recommendation, 2011/696/EU*, European Union, Luxembourg, 2011.
12 G. Oberdörster, E. Oberdörster and J. Oberdörster, Nanotoxicology: an emerging discipline evolving from studies of ultrafine particles, *Environ. Health Perspect.*, 2005, **113**, 823.
13 G. Ramachandran, D. Paulsen, W. Watts and D. Kittelson, Mass, surface area and number metrics in diesel occupational exposure assessment, *J. Environ. Monit.*, 2005, **7**, 728.
14 M. Van der Zande, R. J. B. Peters, A. A. Peijnenburg and H. Bouwmeester, Biodistribution and toxicity of silver nanoparticles in rats after subchronic oral administration, *Toxicol. Lett.*, 2011, **205**, S289.
15 R. Peters, Z. Herrera-Rivera, A. Undas, M. van der Lee, H. Marvin, H. Bouwmeester and S. Weigel, Single particle ICP-MS combined with a data evaluation tool as a routine technique for the analysis of nanoparticles in complex matrices, *J. Anal. At. Spectrom.*, 2015, **30**, 1274.
16 D. Bartczak, P. Vincent and H. Goenaga-Infante, Determination of size-and number-based concentration of silica nanoparticles in a complex biological matrix by on-line techniques, *Anal. Chem.*, 2015, **87**, 5482.
17 W. I. Hagens, A. G. Oomen, W. H. de Jong, F. R. Cassee and A. J. Sips, What do we (need to) know about the kinetic properties of nanoparticles in the body?, *Regul. Toxicol. Pharmacol.*, 2007, **49**, 217.
18 G. Roebben, V. Kestens, Z. Varga, J. Charoud-Got, Y. Ramaye, C. Gollwitzer, D. Bartczak, D. Geißler, J. Noble, S. Mazoua, N. Meeus, P. Corbisier, M. Palmai, J. Mihály, M. Krumrey, J. Davies, U. Resch-Genger, N. Kumarswami, C. Minelli, A. Sikora and H. Goenaga-Infante, Reference materials and representative test materials to develop nanoparticle characterization methods: the NanoChOp project case, *Front. Chem.*, 2015, **3**, 56.
19 A. Nel, T. Xia, L. Mädler and N. Li, Toxic potential of materials at the nanolevel, *Science*, 2006, **311**, 622.
20 D. Walczyk, F. B. Bombelli, M. P. Monopoli, I. Lynch and K. A. Dawson, What the cell "sees" in bionanoscience, *J. Am. Chem. Soc.*, 2010, **132**, 5761.
21 T. N. Shendruk and G. W. Slater, Operational-modes of field-flow fractionation in microfluidic channels, *J. Chromatogr., A*, 2012, **1233**, 100.

22 H. Saveyn, B. De Baets, O. Thas, P. Hole, J. Smith and P. Van der Meeren, Accurate particle size distribution determination by nanoparticle tracking analysis based on 2-D Brownian dynamics simulation, *J. Colloid Interface Sci.*, 2010, **352**, 593.
23 P. J. Wyatt, Submicrometer particle sizing by multiangle light scattering following fractionation, *J. Colloid Interface Sci.*, 1998, **197**, 9.
24 F. Aureli, M. D'Amato, A. Raggi and F. Cubadda, Quantitative characterization of silica nanoparticles by asymmetric flow field flow fractionation coupled with online multiangle light scattering and ICP-MS/MS detection, *J. Anal. At. Spectrom.*, 2015, **30**, 1266.
25 V. Nischwitz and H. Goenaga-Infante, Improved sample preparation and quality control for the characterisation of titanium dioxide nanoparticles in sunscreens using flow field flow fractionation on-line with inductively coupled plasma mass spectrometry, *J. Anal. At. Spectrom.*, 2012, **27**, 1084.
26 J. Wernecke, C. Gollwitzer, P. Müller and M. Krumrey, Characterization of an in-vacuum PILATUS 1 M detector, *J. Synchrotron Radiat.*, 2014, **21**, 529.
27 B. R. Pauw, Everything SAXS: small-angle scattering pattern collection and correction, *J. Phys.: Condens. Matter*, 2013, **25**, 383201.